Study of Loss Mechanisms using Half-Cell Measurements in a Regenerative Hydrogen Vanadium Fuel Cell

H. Hewa Dewage[1*], V. Yufit[1] and N. P. Brandon[1]

*Corresponding author: hmh311@imperial.ac.uk

[1]*Department of Earth Science and Engineering, Imperial College London, South Kensington Campus, SW7 2AZ, UK*

Abstract

The positioning of reference electrodes in redox flow batteries without disturbing the cell operation represents a great challenge. However decoupling anode and cathode processes is crucial in order to fully understand the losses in the system so it can be further optimised. The feasibility of a regenerative fuel cell based on an V(IV)/V(V) electrolyte and hydrogen gas has previously been demonstrated. In this investigation, using electrochemical impedance spectroscopy, the various losses of the cathode, anode and whole cell were established using an alternative reference electrode set-up. The findings showed that the largest irreversible losses under the conditions tested arose from diffusion limitations in the cathode and the effect of vanadium crossover and therefore adsorption onto the platinum layer of the hydrogen electrode leading to higher losses on the anode. These results highlight the potential for further improvement and optimisation of cell design and materials for both electrodes in the Regenerative Hydrogen Vanadium Fuel Cell.

Nomenclature

EIS Electrochemical impedance spectroscopy

CPE Constant phase element

j imaginary number

L inductor

MEA Membrane electrode assembly

OCV Open circuit voltage

PEMFC Proton exchange membrane fuel cellQ Capacitance like parameter

RE Reference electrode

RFB Redox flow battery

RHVFC Regenerative hydrogen-vanadium fuel cell

τ time constant

ω frequency

Z Impedance

Subscript

ads/des adsorption/desorption

ads_Pt adsorption on platinum

CT charge transfer

diff diffusion

2

dl double-layer

s series

1. Introduction

Redox flow batteries (RFBs) also called regenerative fuel cells are one of the promising candidates for large scale energy storage. They offer the ability to convert electrical energy into chemical energy which is stored in external tanks containing two redox couples. The anolyte and catholyte are respectively pumped through the anode and cathode of the electrochemical cell where at discharge the chemical energy is converted back to electrical energy[1]. One of the attractive features of these batteries is their flexibility in decoupling power and energy as the power is determined by the stack size and active surface area of each cell while the energy available depends on the electrolyte volume and concentration[2]. Furthermore, RFBs also present additional advantages such as fast response time (~milliseconds), site independence, low environmental footprint, high depth of discharge, high reliability, high energy efficiency (ca. 85%) and long life cycle (> 13 000 cycles) [3–5].

The all-vanadium redox battery (VRB), initially developed by Skyllas-Kazacos, is regarded as one of the most promising RFBs and is already available commercially where it is utilised for load levelling, power quality control and renewable energy deployment [6,7].

Expertise gained on proton exchange membrane fuel cells (PEMFCs) can be applied to RFB research due to their similarities. Accordingly, an increase in hydrogen based hybrid RFBs has been observed in recent years for example with systems such as H_2/Fe, H_2/Br_2, H_2/Ce, as well as the H_2/V discussed here[8–13]. Those systems benefit from the fast kinetics of the hydrogen reaction, and absence of cross-contamination through mixing of liquid anolyte and catholyte.
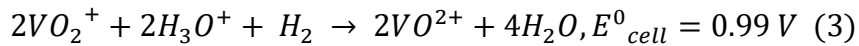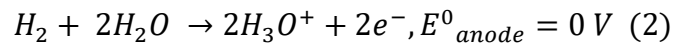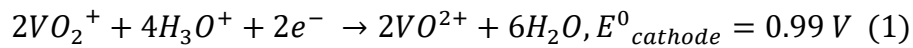
3

While the crossover of the catholyte is still possible, it can be collected on the anode side and pumped back.

In order to decouple the anode and cathode processes, reference electrodes (REs) are usually incorporated into RFB rigs. Similarly to fuel cells, the positioning of a reference electrode in an RFB is not a trivial task due to its gap-free planar cell design. There are currently two main methods of positioning, which are: the "sandwich" (internal) and the "edge" (external) methods. Both of these techniques present drawbacks that might affect the quality and reliability of the measurements. The sandwich method, comprising of the RE placed between two membranes will lead to a larger iR drop, thus also affecting the RE potential reading. Additionally, it will affect charge and water transport in the membrane[14]. In the edge type configuration, the RE is placed in contact with the membrane, outside but as close as possible to the active surface area. This configuration also suffers from many issues such as a non-uniform current may be observed if the RE is placed too close to the electrodes, and the current and potential distribution lines are highly affected by electrode alignment which suggests that a larger error may be found when using two non-identical electrodes [14–16]. Recently Hinds et al. have demonstrated that the challenges faced by the sandwich and edge methods can be minimised by using an alternative RE positioning technique[17]. It consists of setting up an electrolyte bridge, such as a tube is inserted through the end plate, all the way to the membrane electrode assembly (MEA) thus allowing an ionic conductive path between the MEA and the RE placed on the other end of the electrolyte bridge [17].

Electrochemical Impedance Spectroscopy (EIS) has been widely used as a useful technique to assess the losses in electrochemical devices. The mathematical interpretation of EIS results allows the physical understanding of these losses as well as their quantitative and qualitative evaluations[18]. From VRB research, information has been gathered on the whole cell as well as on the cathode using the V(IV)/V(V) redox couple which is of interest in this work. Currently

whole cell EIS analysis fails to decouple contributions from the anode and cathode, while half-cell measurements are generally not gathered in-situ[19,20] However Sun et al. have presented in their work an in-situ EIS study using a dynamic hydrogen reference electrode positioned using the "sandwich" method in the cell[21]. Their results demonstrated that the anode is the limiting electrode in VRBs, contributing most of the losses[21]. Nonetheless the EIS experiments, being carried out under load, could not successfully resolve the cathode processes, the spectra being too distorted[21]. Hence there still remains scope for further in-situ half-cell measurements in VRB and other flow batteries.

The authors have previously presented the feasibility of the regenerative hydrogen-vanadium fuel cell (RHVFC) where in discharge mode, vanadium (V) is reduced to vanadium (IV) at the cathode while hydrogen is oxidised at the anode as described by Equations 1, 2 and 3:
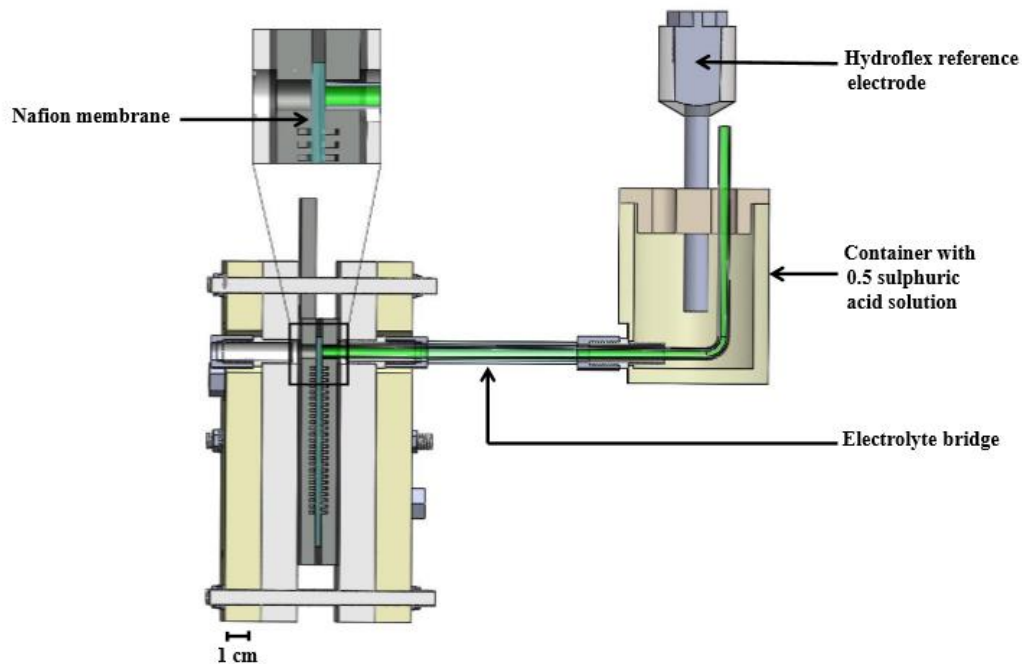
$$2VO_2{}^+ + 4H_3O^+ + 2e^- \rightarrow 2VO^{2+} + 6H_2O, E^0{}_{cathode} = 0.99\,V \quad (1)$$

$$H_2 + 2H_2O \rightarrow 2H_3O^+ + 2e^-, E^0{}_{anode} = 0\,V \quad (2)$$

$$2VO_2{}^+ + 2H_3O^+ + H_2 \rightarrow 2VO^{2+} + 4H_2O, E^0{}_{cell} = 0.99\,V \quad (3)$$

Figure 1: Schematic of the assembled RHVFC with the integration of the reference electrode set-up (*Figure Credit: A. Kavei*).

Moreover the RHVFC performance dependency on choice of electrode material, especially on the cathode was highlighted in that work. Now in order to better understand and assign losses within the cell, it is crucial to be able to accurately decouple the anodic and cathodic processes. Therefore, here we present an alternative way to gain half-cell measurements in RFBs, inspired by the method developed by Hinds et al. as depicted in Figure 1. Using this set-up, the effects of different parameter on the half-cell and whole cell losses were evaluated.

2. Experimental Details

2.1. Vanadium electrolyte preparation

A vanadium catholyte solution (60 mL) of 1M was prepared by adding 14.1g of vanadium sulphate hydrate (Sigma-Aldrich) into 60 mL of 5M sulphuric acid solution (Fluka Analytical). The mixture was left stirring until the solid was completely dissolved.

2.2. Cell assembly

The experiments were carried out using an in-house cell with a 25 cm^2 active surface area. One layer of a carbon electrode (SGL 10 AA, 400 μm) was used on the vanadium side while a platinised carbon paper electrode (Alfa Aesar Hydrogen Electrode, 200 μm, 0.5 mg/cm^2 Pt loading) was used on the hydrogen side. The two electrodes were separated by a Nafion 117 membrane. The vanadium electrolyte and the hydrogen gas were distributed to the respective electrode through multi-channel serpentine flow channel plates (SGL, BMA5 graphite plates) that also served as current collectors. A polypropylene insulating layer (RS Components) followed by aluminium end plates were used in order to ensure homogeneous cell compression. Various layer of Viton® gaskets were used for sealing in the construction. A torque of 9 N.m was applied to each of the 8 bolts used to compress the cell. Finally a collector was connected to the hydrogen side outlet in order to collect any vanadium electrolyte crossover.

2.3. Reference electrode set-up

A schematic of the RHVFC assembly with the RE set-up is shown in Figure 1. The dynamic hydrogen reference electrode Hydroflex (Gaskatel) was placed in a PTFE container containing a 0.5M sulphuric acid solution. The container was connected to the cell via a PTFE tube of 6.4 mm diameter (Cole-Parmer). In order to avoid air bubbles at the membrane interface and ensure that the ion conduction path is undisturbed, a PTFE tube of 4 mm diameter was inserted through the first tubing as shown by the green tube on Figure 1. Then, a solution of 0.5M sulphuric acid was syringed into the smaller tubing, while the RE was in the container, until a stable potential for the Hydroflex reference electrode could be read. The cell may take up to 24 hours to settle

due to the redistribution of pressure in the cell after assembly, and the structural changes of the non-treated carbon electrode on the vanadium side, therefore all half-cell measurements were collected after this equilibration period. A potential deviation for the RE of up to 40 mV would be measured from the expected 0V *vs SHE* which is considered as acceptable for a dynamic hydrogen reference electrode according to literature[22]. Connections were made to enable RE measurements on both the vanadium and the hydrogen side of the RHVFC, though RE measurements were only made on one electrode at a time i.e when collecting half-cell measurements of the anode the RE was placed on the anode side, and vice versa. No diffusion of the 0.5M sulphuric acid solution was observed from the reference electrode assembly at either electrode.

2.4. Electrochemical measurements

2.4.1. Chronopotentiometry tests

Galvanostatic charge/discharge was carried out using a Bio-Logic potentiostat (VSP-300) with a 10A booster running EC-Lab software. Measurements were made using a 4-electrode cell set-up in order to minimise contact resistance losses. Where the working and sense cables were connected to the cathode individually, the counter was connected to the anode and the reference to the reference electrode. The upper and lower cut-off voltages were 1.3V and 1V respectively as calculated by the Nernst equation assuming 99.9% and 0.1% concentration of V(V) and V(IV) at fully charged state and inversely at fully discharged state.

#### 2.4.2. Electrochemical impedance spectroscopy

Electrochemical impedance spectroscopy was carried out on the cell under different conditions. All measurements were taken at open circuit voltage (OCV) in potentiostatic mode with an AC voltage amplitude of 15mV over a frequency range between 200 kHz and 10 mHz. The data collected was fitted to equivalent circuits using ZView software (Scribner Associates).

3. Results and Discussion

3.1 Effect of vanadium flow rate

Using the RE on the vanadium side, half-cell EIS measurements under various vanadium flow rates were collected for the cathode as displayed in the Nyquist plot in Figure 2A. Two semi-depressed circles can be observed where the higher frequency arc was attributed to charge transfer resistances in the cathode, and the lower frequency arc to diffusion losses. From the decreasing diameters of the two semi-circles in the plot, it can be seen that increasing the flow rate of the catholyte leads to a minor decrease in the charge transfer resistance as well as a larger decrease of the diffusion loss. In order to extract quantitative information out of the measurements, they were fitted to the equivalent circuit presented in Figure 2B. In this circuit R_s represents the series resistance of the cathode, then the second element comprising the double-layer capacitor C_{dl} with the resistance R_{CT} in parallel models the charge transfer losses at the cathode. Finally the last element comprising the constant phase element CPE and the resistor R_{Diff} in parallel simulates the diffusion behaviour of the catholyte in the porous electrode.
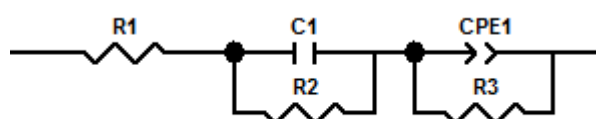
A
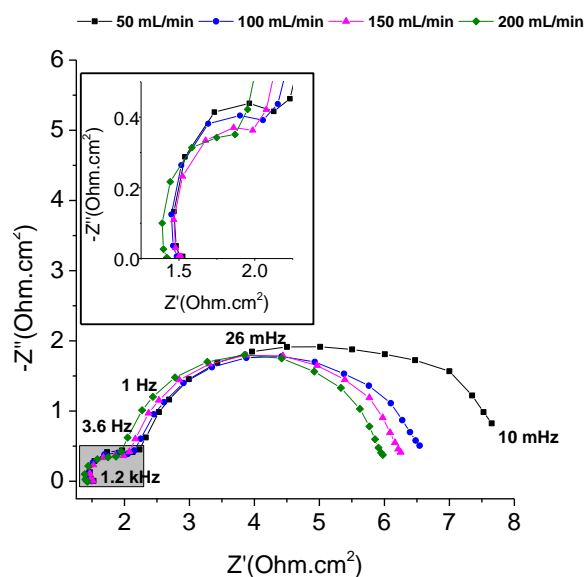
B

Figure 2: A) Nyquist representation of the EIS response of the vanadium half-cell at different vanadium flow rates with a hydrogen flow rate of 100 mL/min. B) Equivalent circuit used to fit the EIS data where R1=R_s, C1=C_{dl}, CPE1=CPE, R2=R_{CT} and R3=R_{Diff}.

The values of the different resistance contributions are presented in Figure 3 where the series resistance (Figure 3A) of the cathode is mostly independent of the vanadium flow rate, except at 200ml/min where a small decrease can be observed. The charge transfer resistance of the cathode process decreases slightly with increasing vanadium flow rate, with a decrease of 13% observed between 50 ml/min and 200 ml/min. The change of flow rate mainly affects the diffusion related resistance, which, as expected, goes down, with increasing flow rate. From 50 to 100 ml/min the resistance drops by 23% and there on by 6% and 4% respectively at 150 and

200 ml/min, relative to the previous value. The total cathode resistance is highest at the lowest flow rate, at which mass transport losses are the largest, contributing nearly 75% (6.0 $\Omega.cm^2$) of the total losses (8.0 $\Omega.cm^2$) at 50 ml/min (Table 1). The total resistance drops by 17% (2.7 $\Omega.cm^2$ difference) from 50 to 100 ml/min followed by a decrease of 5% (0.3 $\Omega.cm^2$ difference) for the following flow rates.
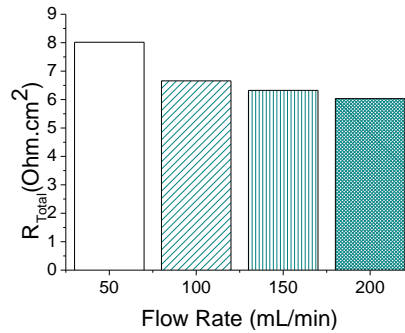
A
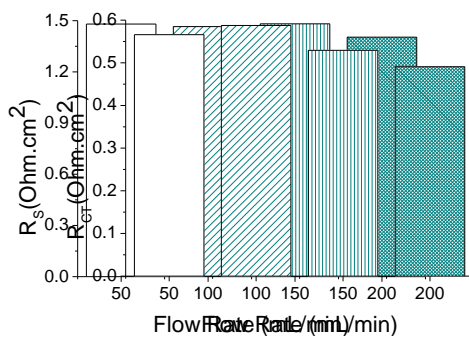
B

C
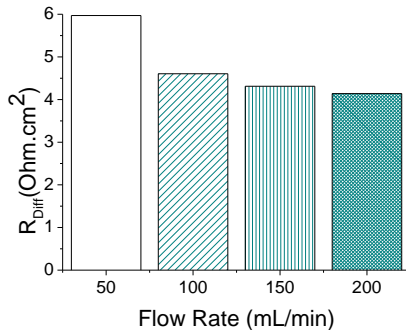
D

Figure 3: A) Series B) Charge transfer C) Diffusion D) Total, resistance of the cathode at different vanadium flow rates and at 100 mL/min hydrogen flow rate.

From this equivalent circuit model, a mathematical expression was derived as presented in Equation 4. The time constants associated with the charge transfer process and the diffusion losses can be calculated from $\tau_{CT} = C_{dl}R_{CT}$ and $\tau_{Diff} = \sqrt[\alpha]{QR_{Diff}}$ where, when α is usually

in the range between 0 and 1 and describes capacitance-like behaviour of non-uniform and porous interfaces. The values of the different parameters can be found in Table 1.

$$Z_{cathode} = R_s + \frac{R_{CT}}{1 + j\omega C_{dl} R_{CT}} + \frac{R_{Diff}}{1 + (j\omega)^\alpha Q R_{Diff}} \quad (4)$$

The τ_{CT} values in Table 1 are in the order of a few milliseconds which is close to the values obtained by Yufit et al. from whole cell measurements of the RHVFC[12]. The values of τ_{Diff} are also consistent with previous work. It can be noted that τ_{CT} increases with increasing flow rate whereas τ_{Diff} decreases.

Table 1: Time constants values for the circuit elements used to fit the vanadium half-cell and whole cell EIS spectra at different vanadium flow rates.

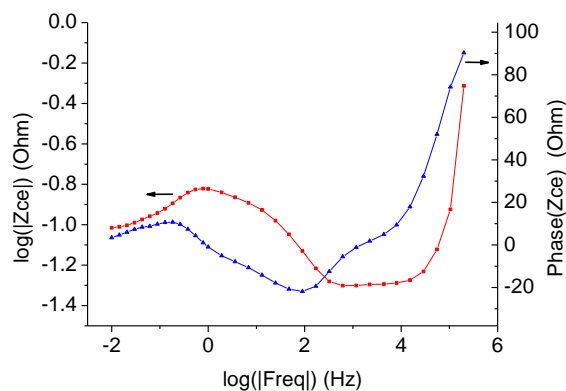|	Vanadium Flow Rate (mL/min)				Hydrogen Flow Rate (mL/min)			
	50	100	150	200	25	50	75	100
Vanadium Half-Cell								
Contribution of Rs (%)	18	22	24	23	22	22	22	22
Contribution of RCT (%)	7	9	8	8	10	9	10	10
Contribution of Rdiff (%)	75	69	68	69	68	68	68	68
Total Resistance (Ω.cm²)	8.02	6.66	6.32	6.03	6.57	6.47	6.36	6.28
τCT (ms)	8.25	8.75	9.00	9.00	7.60	7.47	7.55	7.52
τDiff (s)	1.28	0.86	0.74	0.66	1.21	1.22	1.21	1.23
Hydrogen Half-Cell								
Contribution of Rs (%)	30	33	35	36	36	36	36	36
Contribution of Rads/des (%)	51	33	23	19	50	54	55	56
Contribution of RPtads (%)	19	34	42	45	14	10	9	8
Total Resistance (Ω.cm²)	4.08	3.73	3.41	3.30	3.61	3.60	3.60	3.64
Whole Cell								
Contribution of Rs (%)	47	56	58	59	55	55	56	55
Contribution of RCT (%)	2	2	2	2	2	2	2	2
Contribution of Rdiff (%)	51	42	40	39	43	43	42	43
Total Resistance (Ω.cm²)	11.4	9.35	8.50	8.04	9.86	9.78	9.64	9.76
τCT (ms)	0.11	0.15	0.21	0.23	0.17	0.16	0.17	0.15
τDiff (s)	1.20	0.59	0.45	0.39	1.00	1.02	0.99	1.02

A
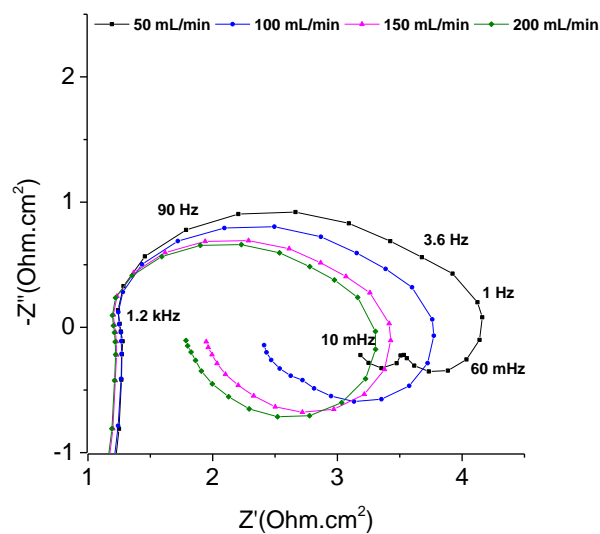
B
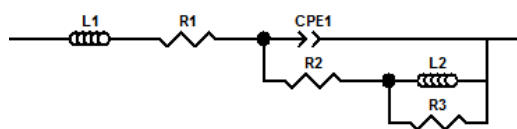
C

Figure 4: A) Nyquist representation of the EIS response of the hydrogen half-cell at different vanadium flow rates with a hydrogen flow rate of 100 mL/min. B) Equivalent circuit used to fit the EIS data where L1=L_{wires}, R1=R_s, CPE1=CPE, R2=$R_{ads/des}$, L2=L_{ads_Pt}, R3=R_{ads_Pt}. C) Bode plots of the EIS response of the hydrogen half-cell at different vanadium flow rates with a hydrogen flow rate of 100 mL/min.

Using the RE on the hydrogen side, half-cell EIS measurements were collected for the anode as displayed in the Nyquist plot in Figure 4A. The anode half-cell spectra using this RE arrangement leads to different results to those obtained for the cathode. A depressed semi-circle can be observed first. From half-cell studies of fuel cells this can be related to hydrogen adsorption and desorption on the platinum in combination with charge transfer that cannot be resolved[23]. Mass transport limitations due to diffusion of molecular hydrogen through porous media are considered to be negligible as the process is too fast to be detected[23]. Then at lower frequencies, an inductive loop occurs, from adsorption studies on the behaviour of PEMFC cathodes it can be concluded that this probably represents an adsorption of crossing vanadium ions onto the platinum catalyst[23–25].
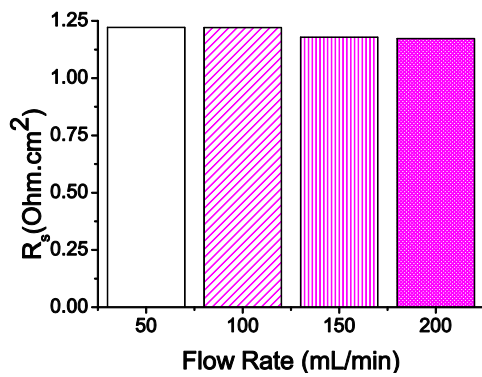
Increasing the flow rate of the catholyte leads to a decrease of the hydrogen adsorption/desorption resistance; as can be deducted from the decreasing diameters of the first semi-circles in the plot. This behaviour can be attributed to the higher crossover of protons transported to the anode. Subsequently the vanadium adsorption resistance on the platinum catalyst increases; further confirming a strong correlation between crossover and flow rate. Also at lower flow rates two inductive loops can be seen that would suggest two different processes occurring, however as the flow rate increases they coalesce and can no longer de discerned. At this stage it is difficult to determine the exact mechanism of the two adsorption processes, and this requires further investigation. The data was fitted to the equivalent circuit presented in Figure 4B. In this circuit, at high frequencies, L_{wires} represents the inductive behaviour of the wires and R_s represents the series resistance of the anode. The constant phase element CPE and its corresponding parallel resistance $R_{ads/des}$ model hydrogen adsorption/desorption onto the platinum catalyst. Finally the last element comprising L_{ads_Pt} and R_{ads_Pt} in parallel describes vanadium adsorption onto the platinum catalyst. The L_{ads_Pt} was chosen to model the low frequency inductive behaviour at the anode because an inductive

14

behaviour arises when the current and the voltage perturbation present a characteristic positive phase shift, as can be observed in the Bode plots in Figure 4C[18,26]. . It has been suggested that the vanadium adsorbed intermediate coverage and its change in coverage when a potential perturbation is applied is slow[18,26]. Hence there is a delay between the time of the perturbation and the time for the current to stabilise[18,26]. This delay is the origin of that positive phase shift[18,26]. The mathematical expression for this equivalent circuit has been derived, as shown in Equation 5, however due to the interdependency of the second and third elements, it is not possible to calculate the time constants for the hydrogen and vanadium adsorption processes.
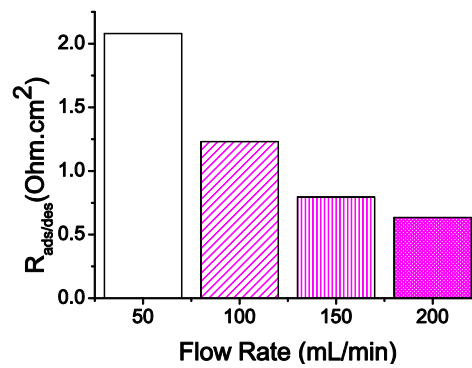
$$Z_{anode} = j\omega L_{wires} + R_s + Z^*, 5A$$

$$Z^* \frac{j\omega L_{ads\_Pt}\left(\frac{R_{ads}}{des} + R_{ads\_Pt}\right) + \frac{R_{ads}}{des}R_{ads\_Pt}}{(j\omega)^{\alpha+1}QL_{ads\_Pt}\left(\frac{R_{ads}}{des} + R_{adsPt}j\omega L_{adsPt}\right) + (j\omega)^{\alpha}Q\left(\frac{R_{ads}}{des}R_{adsPt}\right) + j\omega L_{ads\_Pt} + R_{ads\_Pt}} \quad (5B)$$

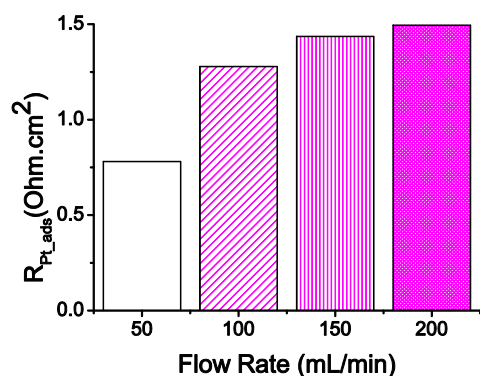A   B
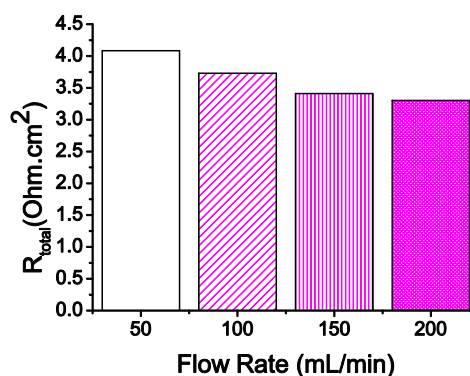

15

C

D

Figure 5: A) Series B) Hydrogen adsorption/desorption C) Vanadium adsorption D) Total, resistance of the anode at different vanadium flow rates and at 100 mL/min hydrogen flow rate.

The individual values of the different resistance contributions as a function of catholyte flow rate are displayed in Figure 5 and their contributions to the total cell resistance is given in Table 1. From Figure 5A, the series resistance of the anode is little affected by the catholyte flow rate, with only a minor decrease observed at higher flow rates. The resistance of $R_{ads/des}$ decreases with increasing catholyte flow rate, whereas the resistance of R_{ads_Pt} increases. These two resistance contributions are in the same order of magnitude. However according to Figure 5D, the total resistance of the anode is higher at lower vanadium flow rate.

A
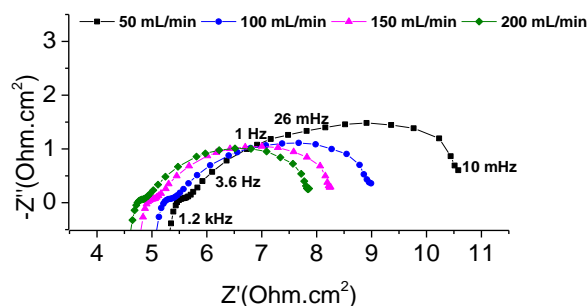
B

Figure 6: A) Nyquist representation of the EIS response of the whole cell at different vanadium flow rates with a hydrogen flow rate of 100 mL/min. B) Equivalent circuit used to fit the EIS data where L1=L, R1=R_s, C1=C_{dl}, R2=R_{CT}, CPE1=CPE and R3=R_{Diff}.

Whole cell EIS data for the RHVFC was also collected when the RE was positioned on the cathode or anode sides. The data collected with RE present on either side, and when there is no RE, matched well. The EIS whole cell spectra at different vanadium flow displayed in Figure 6A show the presence of two depressed semi-circles meaning that there are at least two different processes. Both of these processes could reflect a contribution from the anode and the cathode, however it is believed that the first process at medium range (4.4kHz to 10 Hz) frequencies shows the charge transfer resistance of the hydrogen reaction, whereas the second process at lower frequencies (10Hz to 10mHz) is governed by vanadium diffusion losses. As for the anode and the cathode, the whole cell resistance losses were quantified using an equivalent circuit (Figure 6B) where L represents the inductance behaviour and R_s the sum of all component resistances in the cell. The double-layer capacitor C_{dl} and parallel resistance R_{CT} emulate the charge transfer resistance of hydrogen rather than the adsorption/desorption resistance as seen in the anode spectra. Finally the last element is the constant phase element CPE and R_{Diff} in parallel that describes the vanadium mass transport related losses.

Equation 6 gives the expression of the total cell impedance and its related time constants are given in Table 1. The low value of tenth of milliseconds of τ_{CT} matches that measured for hydrogen charge transfer in PEMFCs found in the literature[27]. Moreover, τ_{Diff} is of the same

order as the diffusion process time constant of the cathode discussed earlier. However it is not yet understood why the charge transfer process of hydrogen cannot be resolved in the anode half-cell spectra, nor why the charge transfer of vanadium does not seem to contribute more significantly to the medium frequency range of the whole cell spectra.

$$Z_{whole\ cell} = j\omega L + R_s + \frac{R_{CT}}{1 + j\omega C_{dl}R_{CT}} + \frac{R_{Diff}}{1 + (j\omega)^\alpha Q R_{Diff}} \quad (6)$$
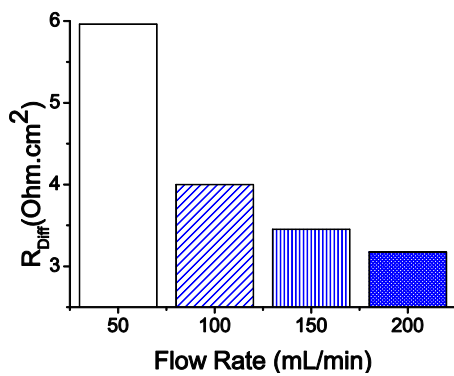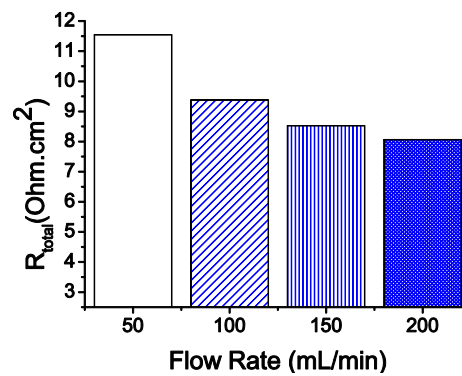
A
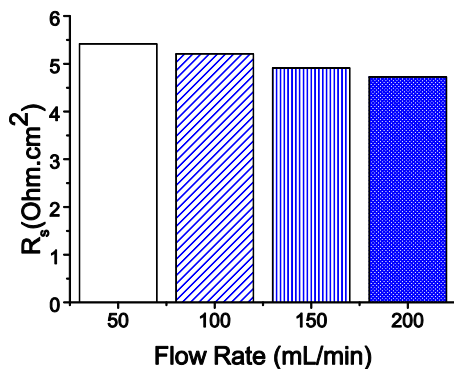
B
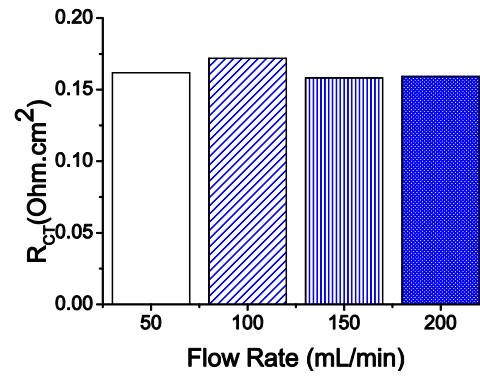
C

D

Figure 7: A) Series B) Hydrogen charge transfer C) Vanadium diffusion D) Total resistance of the whole cell at different vanadium flow rates and at 100 mL/min hydrogen flow rate.

It can be observed that the series resistance of the cell decreases slightly as the flow rate of the catholyte increases (Figure 7A). A possible explanation is that the membrane becomes more hydrated at higher flow rates therefore experiencing a decrease in resistance The hydrogen charge transfer process resistance is fairly constant regardless of the flow rate. Therefore, under the conditions tested, the biggest contribution to the total losses of this cell is the diffusion resistance (Figure 7C). In the whole cell spectra, similar to the cathode spectra, the resistance decreases as the flow rate increases. Overall it is observed that the total cell resistance becomes smaller as the vanadium flow rate increases.
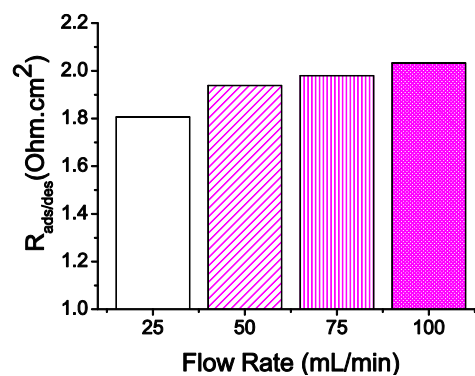
3.2 Effect of hydrogen flow rate

EIS data at OCV was collected at a constant vanadium flow rate with varying hydrogen flow rates. The response of the cathode and the whole cell did not seem affected by varying this parameter, as demonstrated by the different resistance contributions presented in Table 1. Only the anode revealed small changes in the resistances values, as can be seen in Figure 8. This is to be expected as it was established from previous work, and from these decoupled experiments[12]. As discussed, it is the vanadium cathode diffusion, which is the largest loss contribution under the conditions tested in this system.
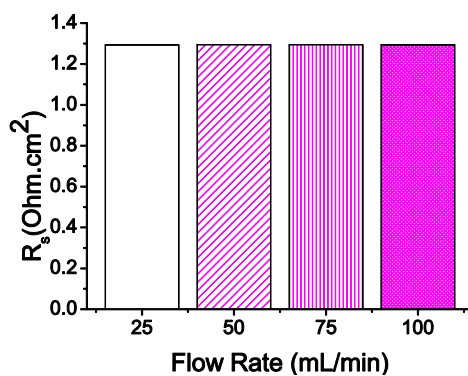
A   B
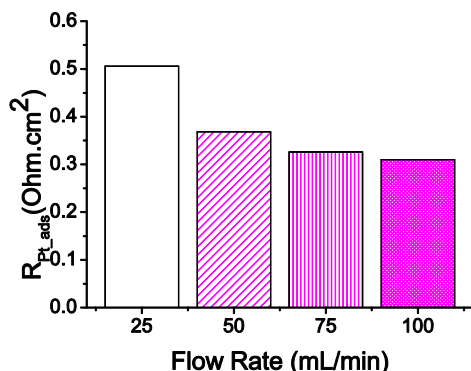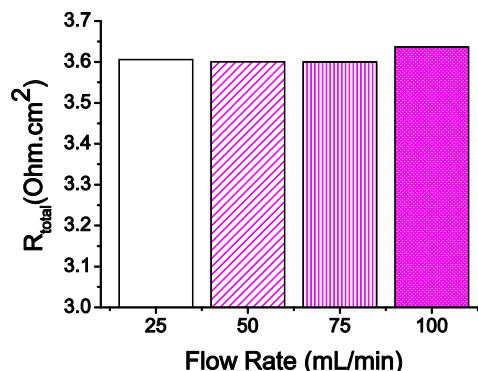
C   D

Figure 8: A) Series B) Hydrogen adsorption/desorption C) Vanadium adsorption D) Total, resistance of the anode at different hydrogen flow rates and at 100 mL/min vanadium flow rate.

It is clear that the hydrogen flow rate has little or no effect on the series resistance of the anode (Figure 8A). However the hydrogen adsorption/desorption process (Figure 8B) seems to have an increasing resistance as the flow rate goes up, while the effect of vanadium adsorption on the platinum catalyst reduces with increased flow rate (Figure 8C). The difference of each resistance contribution between 25 and 100 mL/min is 6% nonetheless the overall cell resistance is slightly higher at 100 mL/min. Looking at the values from Table 1 and Figure 8D, while a small gain can be achieved if operating the cell at 50 or 70 mL/min, the improvement is not that significant when compared to the effect of vanadium electrolyte flow rate.

4. Conclusion

The feasibility of an alternative RE set-up, adapted from Hinds et al., was demonstrated for RFBs. This allowed the decoupling of anode and cathode processes measurements without altering the cell behaviour and the obtained data could be fitted using equivalent circuit models providing a physical meaning to the different processes 17. Parameters from the equivalent circuit fitting were extracted with on average less than 15% error, and with a maximum error

20

of 40% for one parameter. This preliminary half-cell EIS study at OCV showed the reliability of this set-up. From the experiments it was deducted that cathode diffusion losses are the largest contribution to the RHVFC along with ohmic losses. Moreover it was also observed that vanadium crossover to the anode could be detected through vanadium adsorption onto the platinum catalyst. Finally, the insignificant effect of hydrogen flow rate in comparison to the effect of the catholyte flow rate has been demonstrated.

This suggests that further work is required into minimising vanadium crossover through improved ion selectivity of the membrane. Future studies should also look into optimising the cathode electrode structure to enhance mass transport to and within the electrode. It is essential to improve cell design for the next RHVFC generation in order to minimise high ohmic losses due to poor current collection, as are experienced here. Such a cell would deliver better performance overall and EIS under load tests would inform about the losses under such conditions.

1. M. Bartolozzi, *J. Power Sources*, **27**, 219–234 (1989).

2. M. Rychcik and M. Skyllas-Kazacos, *J. Power Sources*, **22**, 59–67 (1988).

3. M. Skyllas-Kazacos, M. H. Chakrabarti, S. a. Hajimolana, F. S. Mjalli, and M. Saleem, *J. Electrochem. Soc.*, **158**, R55 (2011).

4. S. Eckroad, *Handbook of Energy Storage for Transmission or Distribution Applications.* Electric Power Research Institute, Editor, California (USA), (2002).

5. C. Ponce de León, A. Frías-Ferrer, J. González-García, D. A. Szánto, and F. C. Walsh, *J. Power Sources*, **160**, 716–732 (2006).

6. M. Skyllas-Kazacos, *J. Electrochem. Soc.*, **133**, 1057 (1986).

7. K. C. Divya and J. Østergaard, *Electr. Power Syst. Res.*, **79**, 511–520 (2009).

8. M. Alon, A. Blum, and E. Peled, *Feasibility study of hydrogen/iron redox flow cell for grid-storage applications*, p. 417-420, (2013).

9. K. Fatih, D. P. Wilkinson, F. Moraw, A. Ilicic, and F. Girard, *Electrochem. Solid-State Lett.*, **11**, B11 (2008).

10. M. C. Tucker, V. Srinivasan, P. N. Ross, and A. Z. Weber, *J. Appl. Electrochem.*, **43**,

637–644 (2013).

11. K. T. Cho et al., *J. Electrochem. Soc.*, **159**, A1806–A1815 (2012).

12. V. Yufit, B. Hale, M. Matian, P. Mazur, and N. P. Brandon, *J. Electrochem. Soc.*, **160**, A856–A861 (2013).

13. H. Hewa Dewage et al., *J. Mater. Chem. A*, **3**, 9446–9450 (2015).

14. G. Li and P. G. Pickup, *Electrochim. Acta*, **49**, 4119–4126 (2004).

15. J. H. Ohs, U. Sauter, S. Maass, and D. Stolten, *J. Electrochem. Soc.*, **159**, F181–F186 (2012).

16. Z. Liu, J. S. Wainright, W. Huang, and R. F. Savinell, *Electrochim. Acta*, **49**, 923–935 (2004).

17. G. Hinds and E. Brightman, *Electrochem. commun.*, **17**, 26–29 (2012).

18. P. Piela, R. Fields, and P. Zelenay, *J. Electrochem. Soc.*, **153**, A1902 (2006).

19. J. N. Noack, L. Vorhauser, K. Pinkwart, and J. Tuebke, in *ECS Transactions*,, vol. 33, p. 3–9, The Electrochemical Society (2011).

20. A. Bourke et al., *J. Electrochem. Soc.*, **162**, A1547–A1555 (2015).

21. C.-N. Sun et al., *ECS Electrochem. Lett.*, **2**, A43–A45 (2013).

22. F. S. A. J. Bard, G. Inzelt, *Electrochemical Dictionary*, p. 173, Springer, (2008).

23. H. Kuhn, B. Andreaus, A. Wokaun, and G. G. Scherer, *Electrochim. Acta*, **51**, 1622–1628 (2006).

24. I. A. Schneider, H. Kuhn, A. Wokaun, and G. G. Scherer, *J. Electrochem. Soc.*, **152**, A2092 (2005).

25. V. F. Lvovich, *Impedance Spectroscopy: Applications to Electrochemical and Dielectric Phenomena*, p. 145-146, John Wiley & Sons, (2012).

26. J. T. Müller, P. M. Urban, and W. F. Hölderich, *J. Power Sources*, **84**, 157–160 (1999).

27. O. Himanen, T. Hottinen, M. Mikkola, and V. Saarinen, *Electrochim. Acta*, **52**, 206–214 (2006).